

# Classical novae from the POINT-AGAPE microlensing survey of M31 – I. The nova catalogue<sup>\*</sup>

M.J. Darnley<sup>1</sup>†, M.F. Bode<sup>1</sup>, E. Kerins<sup>1</sup>, A.M. Newsam<sup>1</sup>, J. An<sup>2</sup>, P. Baillon<sup>3</sup>, S. Calchi Novati<sup>4</sup>, B.J. Carr<sup>5</sup>, M. Crézé<sup>6,7</sup>, N.W. Evans<sup>2</sup>, Y. Giraud-Héraud<sup>6</sup>, A. Gould<sup>8</sup>, P. Hewett<sup>2</sup>, Ph. Jetzer<sup>4</sup>, J. Kaplan<sup>6</sup>, S. Paulin-Henriksson<sup>6</sup>, S.J. Smartt<sup>2</sup>, C.S. Stalin<sup>6</sup> and Y. Tsapras<sup>5</sup>

<sup>1</sup>*Astrophysics Research Institute, Liverpool John Moores University, 12 Quays House, Egerton Wharf, Birkenhead, CH41 1LD, UK*

<sup>2</sup>*Institute of Astronomy, University of Cambridge, Madingley Road, Cambridge CB3 0HA, UK*

<sup>3</sup>*CERN, CH-1211 Genève 23, Switzerland*

<sup>4</sup>*Institut für Theoretische Physik, Universität Zürich, Winterthurerstrasse 190, CH-8057 Zürich, Switzerland*

<sup>5</sup>*Astronomy Unit, School of Mathematical Sciences, Queen Mary, University of London, Mile End Road, London E1 4NS, UK*

<sup>6</sup>*Laboratoire de Physique Corpusculaire et Cosmologie, UMR 7553, CNRS-IN2P3 Collège de France, 11 Place Marcelin Berthelot, F-75231 Paris, France*

<sup>7</sup>*Université Bretagne-Sud, Campus de Tohannic, BP 573, F-56017 Vannes Cedex, France*

<sup>8</sup>*Department of Astronomy, Ohio State University, 140 West 18th Avenue, Columbus, OH 43210, USA*

25 May 2004

## ABSTRACT

The POINT-AGAPE survey is an optical search for gravitational microlensing events towards the Andromeda Galaxy (M31). As well as microlensing, the survey is sensitive to many different classes of variable stars and transients. Here we describe the automated detection and selection pipeline used to identify M31 classical novae (CNe) and we present the resulting catalogue of 20 CN candidates observed over three seasons. CNe are observed both in the bulge region as well as over a wide area of the M31 disk. Nine of the CNe are caught during the final rise phase and all are well sampled in at least two colours. The excellent light-curve coverage has allowed us to detect and classify CNe over a wide range of speed class, from very fast to very slow. Among the light-curves is a moderately fast CN exhibiting entry into a deep transition minimum, followed by its final decline. We have also observed in detail a very slow CN which faded by only  $0.01 \text{ mag day}^{-1}$  over a 150 day period. We detect other interesting variable objects, including one of the longest period and most luminous Mira variables. The CN catalogue constitutes a uniquely well-sampled and objectively-selected data set with which to study the statistical properties of classical novae in M31, such as the global nova rate, the reliability of novae as standard-candle distance indicators and the dependence of the nova population on stellar environment. The findings of this statistical study will be reported in a follow-up paper.

**Key words:** novae, cataclysmic variables – galaxies: individual: M31

## 1 INTRODUCTION

Classical novae (CNe) undergo unpredictable outbursts with a total energy that is surpassed only by gamma-ray bursts, supernovae and some luminous blue variables. However, CNe are far more commonplace than these other phenomena (Warner 1989).

CNe are a sub-class of cataclysmic variables (CVs). The

canonical model for CVs (Crawford & Kraft 1956) is that they are close binary systems, generally of short period, containing a low-mass G or K type near-main-sequence late-type dwarf that fills its Roche lobe (the secondary) and a more massive carbon-oxygen or magnesium-neon white dwarf companion (the primary). As the secondary fills its lobe, any tendency for it to increase in size through evolutionary processes causes a flow of material through the inner Lagrangian point into the primary's lobe. The high angular momentum of the transferred material causes it to form a disc around the white dwarf. Viscous forces within this accretion disc act to transfer material inwards, so that a small amount of the accreted hydrogen-rich material falls on to the primary's surface. As this layer grows, the temperature of the material increases. Eventually the tempera-

<sup>\*</sup> Based on observations made with the Isaac Newton Telescope operated on the island of La Palma by the Isaac Newton Group in the Spanish Observatorio del Roque de los Muchachos of the Instituto de Astrofísica de Canarias.

† E-mail: mjd@astro.livjm.ac.uk

**Table 1.** Principal M31 classical nova surveys

Author(s)	Epoch	Filter(s)	Detector	Novae	Annual rate	Reference(s)
Hubble	1909–1927	B	Plates	85	$\sim 30$	1
Arp	1953–1954	B	Plates	30	$24 \pm 4$	2
Rosino <i>et al.</i>	1955–1986	B	Plates	142	-	3, 4, 5
Ciardullo <i>et al.</i>	1982–1986	B, H $\alpha$	CCD	40	-	6, 7
Sharov & Alksnis	1969–1989	B	Plates	21	-	8
Tomaney & Shafter	1987–1989	H $\alpha$	CCD	9	-	9
Shafter & Irby	1990–1997	H $\alpha$	CCD	72	$37^{+12}_{-8}$	10
Rector <i>et al.</i>	1995–1999	H $\alpha$	CCD	44	-	11
Darnley <i>et al.</i>	1999–2002	$r', i', g'$	CCD	20	*	12

References: (1) Hubble (1929); (2) Arp (1956); (3) Rosino (1964); (4) Rosino (1973); (5) Rosino *et al.* (1989); (6) Ciardullo *et al.* (1987); (7) Ciardullo *et al.* (1990); (8) Sharov & Alksnis (1991); (9) Tomaney & Shafter (1992); (10) Shafter & Irby (2001); (11) Rector *et al.* (1999); (12) This work.

\* To be reported in a follow-up paper.

ture may become high enough to initiate hydrogen burning. Given the correct conditions, this can lead to a thermonuclear runaway in which the accreted material (and possibly some of the “dredged-up” white dwarf) is expelled from the system in a nova eruption (King 1989; Starrfield 1989).

CNe exhibit outburst amplitudes of  $\sim 10 - 20$  magnitudes and, at maximum light, display an average absolute blue magnitude of  $M_B = -8$  with a limit of around  $M_B = -9.5$  for the fastest (Shara 1981; Warner 1989). They are potentially useful as standard candles for extragalactic distance indication, as they exhibit a correlation between their luminosity at maximum light and the rate of their decline (Hubble 1929; McLaughlin 1945; Arp 1956). Unfortunately, poor light-curve coverage, small sample sizes and a current lack of understanding of how the properties of CNe vary between different stellar populations, have limited their usefulness in this context. Due to their relatively high frequency, novae may also be used as a tool for mapping the spatial distribution of the population of close binary systems in nearby galaxies. Despite the high luminosities of CNe, our position within the Galaxy prevents us from directly observing more than a small fraction of Galactic CNe that erupt each year (Shafter 1997). Therefore the Galactic nova rate is poorly known, with estimates ranging from  $11 \text{ yr}^{-1}$  (Ciardullo *et al.* 1990) to  $260 \text{ yr}^{-1}$  (Sharov 1972). Fortunately, CNe can be readily identified in external galaxies. Surveys of CNe in M31 have been carried out by Hubble (1929), Arp (1956), Rosino (1964, 1973), Ciardullo *et al.* (1987), Capaccioli *et al.* (1989), Sharov & Alksnis (1991), Tomaney & Shafter (1992), Rector *et al.* (1999) and Shafter & Irby (2001) amongst others. These surveys have resulted in the discovery of around 450 novae and have indicated the global nova rate to be  $\sim 30 - 40 \text{ yr}^{-1}$  (Shafter & Irby 2001). Table 1 summarises the findings of many of these past surveys, with most of the data reproduced from Shafter & Irby (2001). The relatively high nova rate of M31 and its close proximity to our own Galaxy are major advantages of targeting M31 for nova surveys. However, since M31 is nearer edge-on than face-on, the task of distinguishing between possible separate disk and bulge nova populations is difficult, and there remains debate surrounding the distribution and rate of novae within M31. POINT-AGAPE (Pixel-lensing Observations with the Isaac Newton Telescope - Andromeda Galaxy Amplified Pixels Experiment) is searching for gravitational microlensing events against the mostly unresolved stars in M31 (Paulin-Henriksson *et al.* 2003). It uses the wide-field camera (WFC) on the Isaac Newton Telescope (INT) to survey a

**Table 2.** The classification of classical nova light-curves into various speed classes according to the time taken to decrease in brightness by two magnitudes ( $t_2$ ) and their  $V$ -band rate of decline ( $dV/dt$ ) from maximum light (Warner 1989).

Speed class	$t_2$ (days)	$dV/dt$ (mag day $^{-1}$ )
Very fast	$\leq 10$	$\geq 0.20$
Fast	11–25	0.18–0.08
Moderately Fast	26–80	0.07–0.025
Slow	81–150	0.024–0.013
Very slow	151–250	0.013–0.008

$0.6 \text{ deg}^2$  region of M31 in at least two broadband filters. The survey has very good temporal sampling over the M31 observing season (August – January) for three seasons and is therefore an excellent database within which to look for novae. Whilst H $\alpha$  observations have been shown to be a particularly helpful diagnostic for CN identification (Payne-Gaposchkin 1957; Ciardullo *et al.* 1983), the excellent sampling of our survey more than makes up for an absence of H $\alpha$  data as it allows us to classify the light-curve profiles of different novae.

A commonly used method of describing the overall timescale of an eruption and classifying CNe, is the concept of the nova “speed class”, developed by McLaughlin (1939) and Bertaud (1948). Their definition of the various nova classes depends on the time taken for a nova to diminish by three magnitudes below maximum light,  $t_3$ . Throughout this paper we will use the speed-class definition, modified by Payne-Gaposchkin (1957) for  $t_2$  times, given by Warner (1989), reproduced in Table 2. The 2.5-year baseline of our survey, along with the high sampling rate, allows us to classify novae over a wide range of speed classes.

In order for robust statistical statements to be made about CN populations in external galaxies it is important to take account of the bias induced by the unresolved galactic surface brightness component, which in the inner regions of galaxies may mask much of the CNe light-curve evolution, making identification and classification more difficult. One approach to this is to make the selection procedure for CN candidates completely automated (Darnley *et al.* 2002), so that the detection efficiency for the various CN light-curve morphologies may be assessed as a function of position objectively through Monte Carlo simulation. This is a far from trivial

**Table 3.** The distribution of each of the three seasons of observations by field and filter band.

Season	$r'$ -band	$i'$ -band	$g'$ -band
	observations North/South	observations North/South	observations North/South
1	105/98	44/36	72/75
2	154/150	144/134	0/0
3	74/70	78/73	0/0

task because the light-curve structure of CNe varies considerably with nova speed class. Automation of the pipeline also requires that, in the absence of  $H\alpha$  observations, the light-curves are well sampled.

The aim of this study is to present the first fully automated search for CN which can be used to assess in an objective manner the statistical properties of the CN population in M31. The study includes some of the finest examples of extragalactic nova light-curves observed to date. In a companion work we will study the spatial distribution and rate of novae in M31. We will also assess the potential of our nova candidates as distance indicators by calibrating the maximum-magnitude versus rate-of-decline and and other proposed relationships (Buscombe & de Vaucouleurs 1955).

The outline of this paper is as follows. In Section 2 we describe the POINT-AGAPE survey dataset. In Section 3 we detail the initial data reduction stages. Section 4 describes the main nova detection pipeline used to define our CN catalogue. The catalogue itself is presented in Section 5 and we discuss our main findings in Section 6.

## 2 THE POINT-AGAPE DATASET

Between the end of 1999 August and the end of 2002 January, we have used the WFC on the INT in La Palma to regularly monitor two fields positioned north and south of the M31 centre and covering  $0.6 \text{ deg}^2$ . The north field is located at  $\alpha = 0^{\text{h}}44^{\text{m}}00^{\text{s}}.0$ ,  $\delta = +41^{\circ}34'00''.0$  and the south field at  $\alpha = 0^{\text{h}}43^{\text{m}}23^{\text{s}}.0$ ,  $\delta = +40^{\circ}58'15''.0$  (J2000), with respect to the centre of CCD4. The WFC consists of a mosaic of four  $2048 \times 4100$  pixel CCDs, and the field locations are indicated in Figure 1. The field placements were primarily chosen to be sensitive to compact dark matter candidates, or Machos, which are predicted to be most evident towards the far side of the M31 disk (Kerins et al. 2001).

The observations were conducted over three seasons in at least two broad-band Sloan-like pass-bands (usually  $r'$  and  $i'$ , though sometimes augmented by  $g'$ ). The three seasons of  $r'$  data comprise 333 epochs from the northern field and 318 epochs from the southern field. The full distribution of observations, in each band, over the three seasons can be seen in Table 3, whilst a graphical representation of the temporal coverage of the northern-field data may be seen in Figure 2.

## 3 DATA REDUCTION

### 3.1 Image pre-processing and alignment

The data pre-processing is performed using the WFC reduction package WFCRED, the processing stages of which include:

- (i) linearity correction;

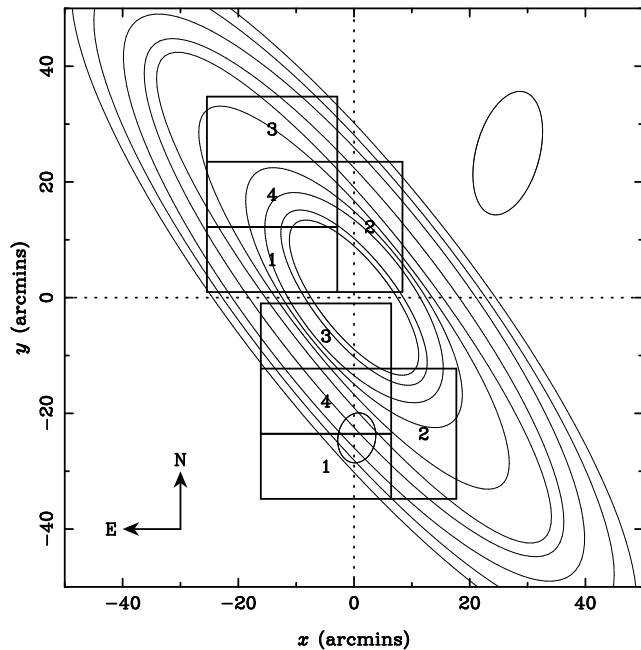


**Figure 1.** The positions of the North and South POINT-AGAPE fields. Each rectangle represents one of the four WFC CCDs and are numbered accordingly. The origin is the centre of M31 at (J2000)  $\alpha = 0^{\text{h}}42^{\text{m}}44^{\text{s}}.324$ ,  $\delta = +41^{\circ}16'08''.53$  (Crane et al. 1992). Also indicated are ten representative M31 “isophotes” from the surface photometry of de Vaucouleurs (1958), along with representations of the positions and sizes of M32 (within the southern field) and NGC205.

- (ii) CCD processing – including de-biasing and flat fielding;
- (iii) de-fringing – for  $i'$  images it is necessary to subtract a mean “fringe frame” to correct for fringing effects; and
- (iv) world coordinate system definition.

After pre-processing, the data reduction steps below are carried out by automated scripts from within the NOAO IRAF package environment<sup>1</sup>.

The first step involves geometrically aligning the image stack. This is carried out using three packages: `xyxymatch` to produce lists of matched reference coordinates; `geomap` to calculate second-order geometric transformations between images; and `geotran` to apply the geometric transforms to the images. The aligned images are then trimmed to produce a common overlap region. The data loss due to the trimming process is summarised in Table 4. Overall it accounts for a loss of 4.5% of the initial data.

### 3.2 PSF matching and background subtraction

The next stage in the reduction process is to match the point-spread functions (PSFs) of the  $r'$  images. The data reduction and candidate selection is performed initially in  $r'$  as this dataset has the best temporal coverage. The `psfmeasure` package is applied to a list of secondary standards (Magnier et al. 1992; Haiman et al. 1994) in order to compute their Gaussian full-width half-maximum (FWHM) on the INT frames. We then select a reference image for

<sup>1</sup> IRAF is distributed by the National Optical Astronomy Observatories, which are operated by the Association of Universities for Research in Astronomy, Inc. under cooperative agreement with the National Science Foundation.

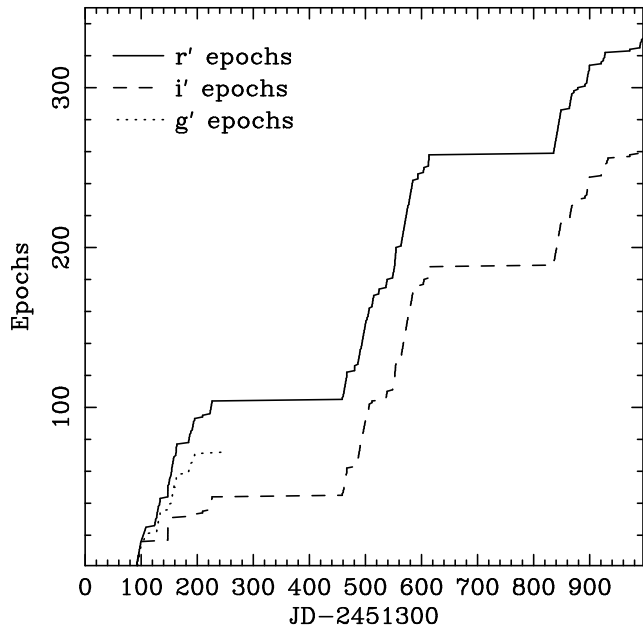


**Figure 2.** The cumulative temporal coverage of the POINT-AGAPE survey in the  $r'$ ,  $i'$  and  $g'$  bands for the northern field. The Southern-field data-set has a similar distribution.

each of the CCDs with an average FWHM closest to, but less than, 1.67 arcsec (5 WFC pixels). Any images exhibiting a poorer seeing than 5 pixels are removed at this stage (accounting for  $\sim 10$  images per CCD). Images that show high ellipticity in their PSFs, further effects of bad atmospheric conditions or instrumental/software deficiency are also removed from the process. Around 10–20 images per CCD are removed for these reasons. The aligned images then have their PSFs matched to that of the reference image using a PSF kernel size that contains 90% of the flux of objects in the reference image. The matching is carried out by applying `psfmatch` to a list of stars selected from the Magnier et al. catalogues which have good PSFs and are resolved in all the images.

An estimate of the background (including the unresolved M31 light) is produced for each PSF-matched image to enable background subtraction. The background image is constructed by passing a  $49 \times 49$  pixel sliding filter, using IRAF’s `median` function. Within the data there are a significant number of pixels that contain counts arising from the extended diffraction structure of saturated sources within, or close to, the observed fields. Image masks are therefore constructed to identify these regions to the detection pipeline. A 24 pixel border around each CCD is excluded as the `median` function does not work reliably near the edges of images. The masks account for a further loss of 4.5% of the data. Table 4 summarises the amount of data lost.

#### 4 CLASSICAL NOVA DETECTION PIPELINE

After aligning and matching the  $r'$  images, they are fed into our nova detection pipeline. The pipeline is written in C and C++ using standard Unix/Linux libraries and the CFITSIO and CCFITS libraries. A flowchart of the pipeline, including the major steps and selection criteria, as discussed in this section, is shown in Figure 3.

**Table 4.** Data lost due to the trimming of the aligned images and the masking of regions of bad data.

CCD	% lost by trimming	% lost by masking	Total % lost
North 1	4.57%	4.23%	8.80%
North 2	4.80%	3.89%	8.69%
North 3	4.25%	4.27%	8.52%
North 4	3.89%	4.96%	8.85%
South 1	3.37%	3.68%	7.05%
South 2	4.96%	7.18%	12.14%
South 3	5.01%	4.65%	9.66%
South 4	5.51%	5.58%	11.09%

#### 4.1 Standard star selection

In order to detect objects which vary in flux, the first step in our pipeline is to prepare a list of resolved standard stars which are known not to vary in luminosity throughout the observations. We later calibrate the light-curves of our CN candidates relative to these stars to eliminate any seeing effects in the data. This selection is carried out using the secondary standard stars from the Magnier et al. BVRI catalogues of M31 (Magnier et al. 1992; Haiman et al. 1994), which contain 485,425 objects. As the catalogues make use of a different filter system from that used by our survey, we must later use data provided by the Cambridge Astronomical Survey Unit (CASU) INT Wide Field Survey (WFS) to accurately calibrate our magnitude scales. However, for the purpose of relative calibration of the candidate light-curves, we initially use a fiducial zero point of  $r' = 25$  to provide a rough estimate of the magnitude scale of our data.

Candidates for non-varying stars are selected from the Magnier et al. catalogues by virtue of their type (i.e. stars), reliability and apparent magnitude. Light-curves for each of the standard stars are then produced using aperture photometry. Standard stars that contain any points in their light-curves which correspond to saturated pixels in any observation are immediately eliminated. To define a sample of standards which do not vary over the survey lifetime, we firstly make the assumption that any variation in flux is due entirely to extraneous factors such as seeing variations. Then, for each epoch, we calculate the mean flux correction such that the stars have statistically the same flux as measured in the reference image. We then test the initial assumption that all the selected stars do not vary. We fit each standard star with a constant-flux light-curve. If any of the standard stars have fits with a reduced- $\chi^2 > 3$ , then the star exhibiting the poorest fit is assumed to have varied in flux. This process is iterated, removing the star with the poorest fit, re-computing the statistical correction and refitting the light-curves until all of the remaining stars have a reduced- $\chi^2 \leq 3$ .

#### 4.2 Object definition

To produce an initial list of CN candidates, we first create a list of “objects” for each observation epoch. We define an object to be a resolved structure in a PSF-matched image with a flux at least  $10\sigma$  above the corresponding local median background flux. The flux difference is designated to be the object flux. Our object detection routine, based upon the IRAF `daofind` package, allows us to deal with the strongly varying background and uses median-filtered images to estimate the local background.

We eliminate any objects from the candidate list if they do

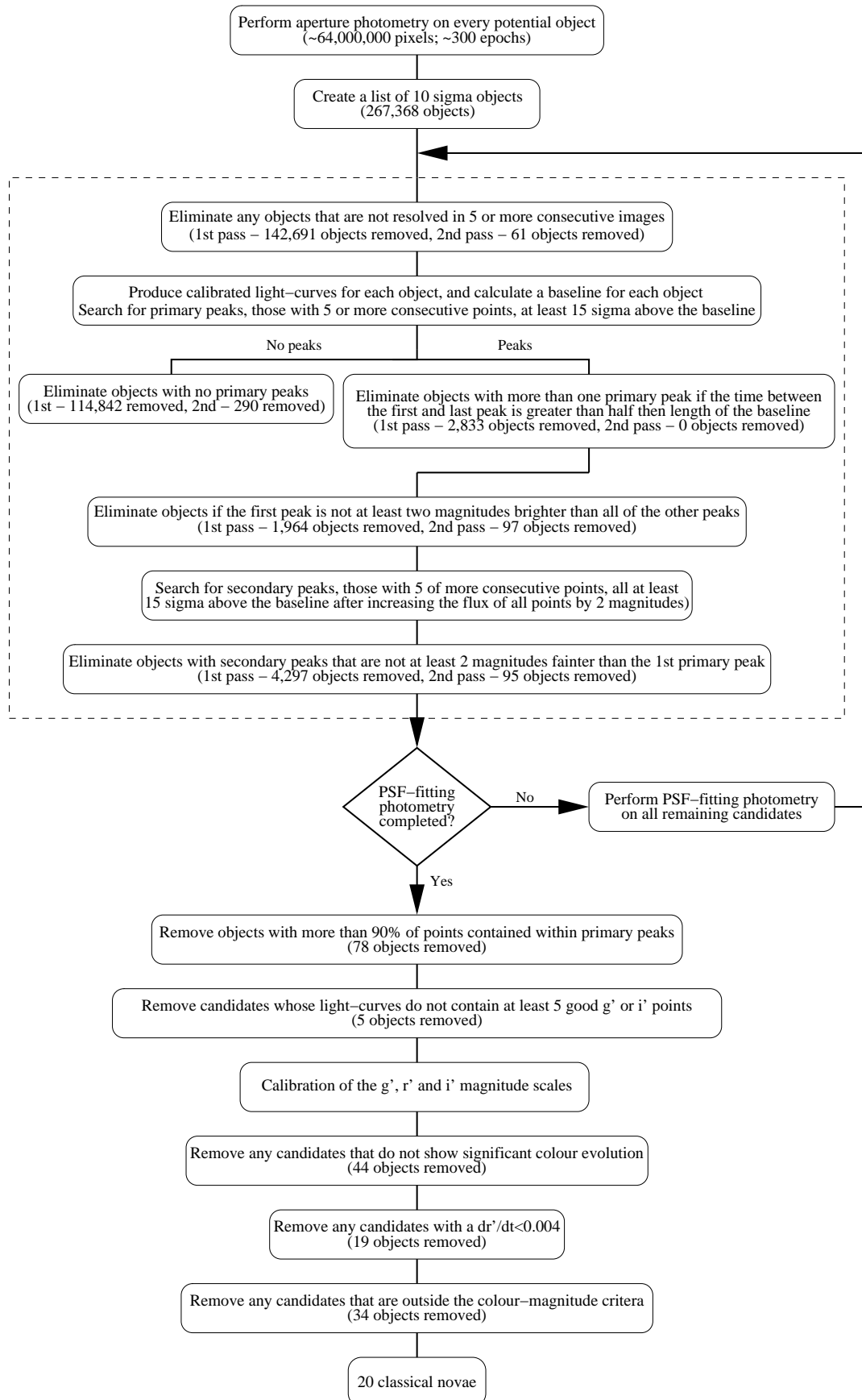


Figure 3. A schematic diagram summarising our classical novae detection process.

not have  $10\sigma$  detections for at least five consecutive observations. This allows us to eliminate from our candidate list any rapidly variable objects (which are unlikely to be novae), cosmic rays, contamination from bad pixels and many of the effects of the extended structure of unmasked saturated objects. When comparing objects between different images, some leeway is needed in the position of the objects to allow for alignment and centring errors. We allow  $\pm 1$  pixel for the maximum error in our custom centring algorithm and  $\pm 0.5$  pixels for the maximum error in the image alignment. In fact the majority of the images are aligned to within  $\pm 0.1$  pixels across the CCD. Thus we treat objects on different frames which are positioned to within  $\pm 2$  pixels as the same object. Giving this amount of leeway results in a small number of multiple detections arising from nearby contaminating variable sources, particularly when the contaminants are bright. However these duplications are easily identified and removed at a later stage.

### 4.3 Preliminary nova selection

We aim to define a set of selection criteria which are general in the sense of not making unnecessary assumptions about CN light-curve morphology, since we want to minimise the risk of biasing against the detection of certain CN speed classes in favour of others. Our starting point is the catalogues of Galactic nova light-curves compiled by Duerbeck (1981) and van den Bergh & Younger (1987) and the “ideal light-curve” (McLaughlin 1960). We wish to derive a set of criteria that allow us to select “CN-like” light-curves from our object list. This is a difficult task since, for example, moderate speed class novae, such as T Aurigae 1891 (McLaughlin 1941) and DQ Herculis 1934 (Adams & Joy 1936), exhibit minima 7 – 10 magnitudes deep during the transition stage. There is also a clear correlation between the morphology of CN light-curves and their rate of decline. These difficulties are further compounded for extragalactic nova detection since it is possible that the transition stage of a moderate speed class nova may be obscured by the host galaxy’s own surface brightness. As a result, these novae may appear to have multiple peaks.

Given the different behaviours of CN light-curves and the extended range of light-curves due to potential contaminating objects, it is not possible, a priori, to define objective selection criteria that are truly effective. Thus, the development of the algorithm used to isolate a sample of CN light-curves involved an iterative process, in which the results of visual inspection of a subset of light-curves surviving each stage in the selection-pipeline were used to refine the selection criteria. To ensure that the objective nature of the selection criteria was preserved, no more than 10% of the candidates surviving at each stage in the selection-pipeline were inspected visually. It was also the case that the feedback from the visual inspection to the refinement of the selection criteria was concerned primarily with reducing the contamination of the CN candidate sample by various classes of variable star. Only at the final stages, where colour cuts are adopted, is it necessary to inspect all the candidates, though by this stage the “obvious” CN candidates are reasonably clearly delineated in magnitude and colour from the other light-curves.

Our first task in the selection is to produce calibrated light-curves for each of the remaining objects in our candidate list. At this preliminary stage the light-curves are produced using aperture photometry and calibrated using the standard stars previously located. For each light-curve we calculate a baseline flux by taking the minimum value obtained from a sliding seven-epoch mean. We also require that the 7 consecutive points which define the baseline each lie within  $3\sigma$  of the baseline value. Windows of 7 points

containing saturated data, or points lying outside the  $3\sigma$  limit, are discarded. If any candidate’s light-curve contains no valid windows (i.e. it isn’t possible to calculate a baseline flux) then that candidate is discarded.

To characterise CN light-curves, we introduce the notion of primary and secondary peaks. CNe can have complex light-curve structures but are generically characterised by an initial large peak (the primary peak) which, in some cases, may be followed by one or more lesser (secondary) peaks. Secondary peaks tend to be at least 2 magnitudes fainter than the primary. The peaks themselves can exhibit some sub-structure and therefore care is required in defining what constitutes a peak.

We define a primary peak as being bounded by points at least  $15\sigma$  above the baseline flux. The other points within the primary peak must either lie at least  $15\sigma$  above the baseline or within  $3\sigma$  of the previous  $15\sigma$  point (in which case they are regarded as “sub-structure” points). A primary peak may contain any number of sub-structure points as long as there are never more than 3 consecutive substructure points. Finally a primary peak must contain at least five points overall. At this stage we are able to discard the majority of candidates as they do not contain any primary peaks. We keep for the moment candidates which contain one or more primary peaks.

For the surviving light-curves we calculate the characteristic width of each primary peak. We define the end of each primary peak as the first point following the peak maximum at which the flux of the object drops below  $3\sigma$  above the baseline, or the final observation if this occurs first. Using a similar definition for the start of each primary peak, we are able to specify the size of each peak. Overlapping primary peaks are then re-assigned as a single primary peak. At this stage, for light-curves with more than one primary peak we require that the time between the maximum flux of the first and last primary peak be less than half the total baseline time of the survey. This criterion is introduced in order to eliminate “contained” periodic variables.

From our studies of a large proportion of all past Galactic nova light-curves, we have noticed that maxima occurring after the transition phase of the nova are always at least two magnitudes fainter than its maximum light. This presents a simple way to eliminate the majority of the multiple primary peak candidates: we require that all primary peaks after the initial one be at least 2 magnitudes below the first peak.

From the remaining light-curves we search for secondary peaks. We define a secondary peak as being 5 or more consecutive points lying at least  $15\sigma$  above the baseline *after increasing the flux of each data point by two magnitudes*. Points already associated with primary peaks are excluded from the search. We then eliminate candidates unless their secondary peaks are at least 2 magnitudes fainter than the first primary peak.

### 4.4 Relative PSF-fitted photometry

The result of the CNe detection pipeline at this stage is a preliminary catalogue of 741 candidates, compared to the 9,835 strongly variable objects (at least one primary peak) originally identified from 267,368  $10\sigma$  objects detected within the two fields. The contaminants within this preliminary catalogue are expected to be mainly long-period variables such as Miras. Further cuts require accurate, multi-colour photometry. This is performed for each surviving candidate in all three colours ( $g'$ ,  $r'$  and  $i'$ ) for all three seasons.

Accurate photometric measurements are obtained by PSF fitting rather than relying on the aperture photometry used until now.

The PSF fitting handles the strongly variable background much more robustly than the simple aperture photometry technique. This is carried out for each of the selected Magnier et al. standards, as well as for the CN candidates. Instrumental magnitudes are extracted using the `psf` and `peak` routines within IRAF’s `daophot` package. After this more accurate calibration, the flux stability of the standards is re-checked using the procedure outlined in Section 4.1. In total we identify 650 standards with stable  $r'$  light-curves, the number of standards per CCD ranges from 9 (South-field CCD2) to 202 (South-field CCD3).

We can now re-apply the criteria previously used in Section 4.3 to eliminate further candidates, taking advantage of the more accurate photometry. This re-processing proves very important in order to remove spurious candidates allowed by aperture photometry. A further 543 candidates are eliminated – more than 70% of the surviving sample. A breakdown of the candidates eliminated at each stage in the pipeline is given in Table 5. The higher photometric reliability allows us to introduce further selection criteria. We require that the light-curves should not have more than 90% of their points in primary peaks. This is essentially a second “containment” criterion which allows us to eliminate long period variables. To investigate colour evolution we further require that the candidates comprise at least 5 points in either  $g'$  or  $i'$ .

#### 4.5 Photometric calibration and colour selections

To calibrate our instrumental  $r'$ ,  $i'$  and  $g'$  magnitudes we used the calibrated zero points for the INT WFC calculated by the CASU WFS team. Their zero points, calculated for many of the nights on which POINT-AGAPE observations were also taken, allow us to test our relative photometry.

Since the colour of CNe is known to vary strongly throughout the eruption (especially just after maximum light), we demand that the  $r' - i'$  and  $g' - r'$  colours of our candidates show significant colour evolution. Accordingly we compute the reduced- $\chi^2$  for a constant colour fit and reject those light-curves where the reduced- $\chi^2 < 3$ . This cut essentially rejects light-curves unless they exhibit colour evolution at a high level of significance.

To eliminate candidates from the catalogue which decay too slowly to be CN, we introduce a rate-of-decline criterion. Using the speed class definitions in Table 2 as a guide, and applying them to the  $r'$  band, we remove light-curves where  $dr'/dt < 0.004 \text{ mag day}^{-1}$  (equivalent to  $t_2 > 500$  days). At this stage we are left with the 52 candidate light-curves which are plotted on the colour-magnitude diagram in Figure 4 which shows  $r'$  at peak versus  $r' - i'$  near peak. Specifically,  $r' - i'$  in Figure 4 represents the mean colour of the object in the magnitude range  $r'_{\text{max}} < r' < r'_{\text{max}} + 3$ . The mean is used in order to average over colour variations near maximum light. In some cases, where the peak flux occurs during poor observing conditions, the mean  $r' - i'$  is better determined than  $r'$  at peak. The candidates are, for the most part segregated into two clumps, one at  $r' \sim 20$ ,  $r' - i' \sim 1.5$  and the other at  $r' \sim 18$ ,  $r' - i' \sim 0$ . If the remaining candidates lie within M31, we expect them to suffer to varying degrees from extinction within that galaxy. However, as the  $r'$  and  $i'$  filters are relatively closely spaced in wavelength, we expect that the change in  $r' - i'$  due to extinction is small, compared to the decrease in both  $r'$  and  $i'$ , and much smaller than the change in  $g' - r'$ . Therefore, the use of colour-magnitude criteria to eliminate further CN candidates is practical. In order to eliminate bogus candidates from the list, we introduce two further criteria:

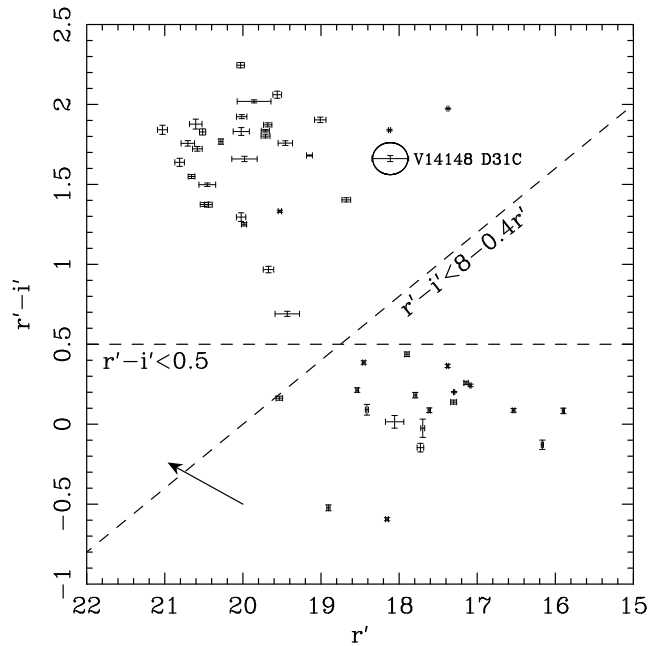


**Figure 4.** A colour–magnitude diagram showing the 52 candidates remaining prior to colour selection. The 20 objects located within the region defined by Equations (1) and (2) are the classical novae discovered by this survey. The group of objects centred at  $r' \sim 20$ ,  $r' - i' \sim 1.5$  appear to be mainly Mira variables. A notable non-nova candidate is indicated, this is discussed in more detail in Section 5.8. The arrow indicates the direction of the reddening vector. The apparent discrepancy in the relative sizes of the  $r'$  and  $r' - i'$  errors seen on some of the points, e.g. V9205 D31C can be understood by considering that the  $r'$  error is drawn solely from the brightest observation (which may have been on a night where no  $i'$  data were taken or when the object was not visible in  $i'$ ) whereas the  $r' - i'$  points, and hence their errors, are drawn from the average colour following maximum light.

$$r' - i' < 0.5 \quad (1)$$

$$r' - i' < 8 - 0.4r' \quad (2)$$

The rationale behind Equation (1) is that we expect novae to have approximately equal brightness in all bands at around maximum, after which they become bluer as the eruption develops. This cut effectively eliminates the clump at  $r' \sim 20$ ,  $r' - i' \sim 1.5$ , which appears mostly to comprise Mira variables. The second colour criterion in Equation (2) is almost orthogonal to the line joining the two clumps and also to the expected direction of the reddening vector indicated in Figure 4. This cut ensures that, whilst we may potentially miss CNe due to reddening, extinction should not cause Miras or similar objects to be mistaken for CNe. This second cut also deals with novae whose maximum light may have been missed; we would expect these novae to appear fainter and bluer. A summary of all of the selection criteria, and their impact for the number of surviving candidates at each stage for each CCD is given in Table 5.

#### 4.6 Astrometry

To calculate the astrometric positions of each CN, we first compute the pixel positions of each nova whilst at or near maximum light using the `apphot center` function. The pixel coordinates of the selected Magnier et al. standards are determined in the reference frames using the `wcsctran` package. Image position solutions

**Table 5.** The effect of each stage of our selection pipeline upon the classical nova catalogue. These steps are described in Section 4.

Pipeline stage	North-field				South-Field				All
	CCD1	CCD2	CCD3	CCD4	CCD1	CCD2	CCD3	CCD4	CCDs
Pixels	$8 \times 10^6$	$8 \times 10^6$	$8 \times 10^6$	$8 \times 10^6$	$8 \times 10^6$	$8 \times 10^6$	$8 \times 10^6$	$8 \times 10^6$	$6.4 \times 10^7$
$10\sigma$ objects	29,423	29,931	39,921	33,125	24,167	28,220	37,086	45,495	267,368
<i>Pipeline 1st pass – aperture photometry</i>									
5 consecutive detections	17,976	15,901	19,292	18,292	12,006	16,258	22,433	20,519	124,677
$\geq 1$ primary peak	1,366	898	1,073	1,215	703	821	2,146	1,613	9,835
Periodicity test	1,036	686	731	908	468	571	1,524	1,078	7,002
Primary peak height	794	539	464	659	318	415	1,126	723	5,038
Secondary peak height	145	77	62	122	37	66	142	90	741
<i>Pipeline 2nd pass – PSF-fitting photometry</i>									
5 consecutive detections	135	66	59	110	35	62	132	81	680
$\geq 1$ primary peak	66	43	38	59	29	44	61	50	390
Periodicity test	66	43	38	59	29	44	61	50	390
Primary peak height	59	33	26	49	16	24	52	34	293
Secondary peak height	35	21	21	35	12	16	37	21	198
<i>Further candidate elimination stages</i>									
$< 90\%$ of points in peaks	22	7	7	21	8	13	29	13	120
$5 g'$ or $i'$ points	22	5	7	20	8	12	28	13	115
Colour evolution	12	4	7	8	5	8	17	10	71
Rate of decline	9	4	5	5	3	5	14	7	52
Colour–magnitude criteria	4	4	1	3	0	0	6	2	20
<b>Final candidates</b>	<b>4</b>	<b>4</b>	<b>1</b>	<b>3</b>	<b>0</b>	<b>0</b>	<b>6</b>	<b>2</b>	<b>20</b>

**Table 7.** M31 classical novae speed class distribution. See Table 2 for the speed class definitions.

Speed class	Number of CN	CN observed before maximum-light
Very Fast	1	0
Fast	3	2
Moderately Fast	11	5
Slow	3	2
Very Slow	2	0

for each CCD are obtained using matched celestial and pixel coordinate lists for the novae within the `ccmap` package to calculate second-order geometric transformations. Finally, the celestial coordinates for each CN are calculated using the computed solutions with the `cctran` package.

## 5 THE CATALOGUE

Following the implementation of our nova detection pipeline and all the candidate selection criteria, we have identified 20 CN candidates. The positions of each of the CNe and further information is tabulated in Table 6. The  $dr'/dt$  parameter is estimated from the general slope of the  $r'$ -band light-curve between the brightest observation and the observation closest to 2 magnitudes fainter than the maximum. The speed class of each CN is then estimated using the definition given in Table 2. However, note that the various speed classes in Table 2 are defined for  $V$ -band light-curves, whilst we are applying them to  $r'$ -band data. Since novae become bluer as they decline, we expect a slight over-estimation of the speeds of the CN relative to the  $V$ -band definitions. Table 7 shows the distribution of our sample of CNe with speed class.

Figures 5 to 9 provide the  $r'$ -band light-curves for each of the

20 CNe discovered and identified in Table 6. Also shown are the  $g' - r'$  and  $r' - i'$  colours, where available. The span of our three observing seasons, and the approximate  $r'$ -band magnitude limit of the PSF fitting are indicated by the horizontal lines in the  $r'$ -band panels. The magnitude limit is determined in the immediate region of each candidate by adding successively brighter artificial PSFs to the data until they are recognised by the PSF-fitting routine. This is performed only on our reference CCD frames (those with a seeing scale closest to 5 pixels), and so represents only an approximate limit for data at other epochs. Where points in the  $r' - i'$  light-curves are apparently “missing” this is usually due to the object being particularly blue. This, coupled with the higher ( $\sim 1$  magnitude) zero-point of the INT CCDs in  $i'$ , means that very blue objects such as novae are often unresolved in  $i'$ -band observations.

The following subsections describe in some detail features of the light-curves of selected CNe from each speed class.

### 5.1 Very fast novae

A lone “very fast” nova was identified by the pipeline, PACN-99-07, which is plotted in Figure 5. The most prominent peak in the  $r'$ -band lightcurve of this CN (occurring around JD  $\simeq$  2451485 days) exhibits a  $dr'/dt = 0.2$  equivalent to a  $t_2 \sim 20$  days. However, this peak appears to be substructure within a broader outburst which seems to have skewed the estimation of the speed class. PACN-99-07 reaches a maximum magnitude of  $r' = 18.1 \pm 0.1$  - much lower than would be expected for a very fast nova at, or near, peak brightness at the distance of M31 (assuming no significant extinction). This, together with the full behaviour of the lightcurve around outburst, leads us to the conclusion that PACN-99-07 is in fact a moderately fast speed class CN.



**Table 6.**

Landscape table to go here.

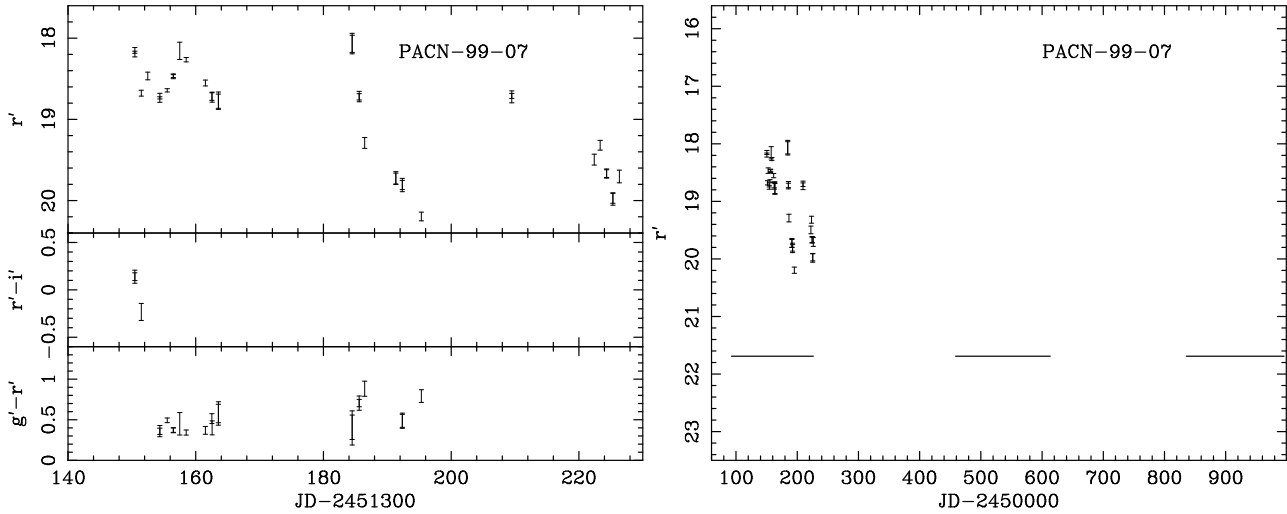


**Figure 5.** A “very fast” nova discovered in M31 from the POINT-AGAPE survey. The left-hand pane shows the  $r'$ -band light-curve around the peak of the nova along with the  $r' - i'$  and  $g' - r'$  colours, where available. The right-hand pane shows the complete  $r'$ -band light-curve over the entire observation period, the horizontal lines indicate the span of our observing seasons and the approximate  $r'$ -band PSF-fitting magnitude sensitivity in the locale of the CN. The automated classification of this CN as very fast arises from the decay rate of the most prominent peak in  $r'$ , occurring around  $\text{JD} \simeq 2451485$  days. Inspection of the full activity around peak indicates that the lightcurve better resembles a moderately fast CN.

## 5.2 Fast novae

As shown in Table 7 and Figure 6, three of the CNe discovered are fast novae, taking between 11 – 25 days to decrease in brightness by two magnitudes from maximum light. Two of these fast CN (PACN-00-06 and PACN-01-02) have been caught in their final rise phase before maximum-light. PACN-99-05 appears to have been first observed at or around maximum.

PACN-00-06 was observed four times during its final rise phase. It was first observed at on 19th October 2000 with  $r' = 18.08 \pm 0.01$ , before rising to  $r' = 17.09 \pm 0.01$  on 21st October. The nova was again observed two weeks later about 1.5 magnitudes fainter. PACN-00-06 was followed for about 4 magnitudes. PACN-00-06 was also observed by the Naini Tal M31 microlensing survey group (Joshi et al. 2004), and was designated by them CN NMS-1.

PACN-01-02 was observed several times before maximum light, first on 15th August 2001. It brightened by 1.3 magnitudes until it reached a maximum-light of  $r' = 17.14 \pm 0.03$  on 21st August. The light-curve was well sampled through maximum-light and into the initial decline phase and was followed for around three magnitudes.

## 5.3 Moderately fast novae

We have discovered eleven moderately-fast novae, those with a  $dr'/dt$  in the range  $0.025 - 0.07 \text{ mag day}^{-1}$ . Their light-curves are shown in Figure 7.

Five of these novae (PACN-99-06, PACN-00-04, PACN-00-07, PACN-01-04 and PACN-01-06) were first seen during their final rise phase, with the remaining novae all appearing to be first observed around or just after maximum-light. Two of the moderately-fast novae (PACN-00-04 and PACN-00-05) exhibit strong oscillations in their light-curves around maximum light, as is expected for some moderately fast novae. PACN-00-05 also shows evidence of a large transition phase minimum between its early and late decline stages, typical of that associated with the rapid formation of an optically thick dust shell in the ejecta (Bode & Evans 1989). The light-curve of PACN-99-06, contains four points in both  $r'$

and  $g'$  during the final rise phase before reaching a maximum of  $r' = 16.17 \pm 0.01$  and  $g' = 16.91 \pm 0.01$ . This CN was first observed on 7th September 1999 with  $r' = 17.36 \pm 0.03$ . When observed again, just over 24 hours later, it had increased in brightness by 0.9 magnitudes. This CN was observed two days later at its maximum-light (11th September), so in the 78 hours prior to maximum-light this CN had increased in brightness by 1.2 magnitudes. We were able to follow PACN-99-06 for about 5 magnitudes below peak. The light-curve of PACN-99-06 appears to show that we have observed the pre-nova and post-nova light for this nova, however this would give this nova a range of only  $\sim 5.5$  magnitudes, highly unlikely for any CN. In fact the points in the light-curve, all at  $r' \sim 21$  are contaminants from a nearby object, whose position is within the errors allowed for each object (see Section 4). When PACN-99-06 is unresolved, at the beginning of the 1st season and for the entirety of the 2nd and last, the PSF-fitting photometry procedures have re-centred upon this nearby object – a relatively faint resolved star in the M31 field.

The nova PACN-00-04 was observed six times before maximum light, first on 8th August 2000 with  $r' = 19.34 \pm 0.06$ , before rising to  $r' = 17.61 \pm 0.03$  just over two days later. A secondary maximum was observed at  $r' = 18.07 \pm 0.03$  on 1st September. This nova was only followed for about 2.5 magnitudes below peak.

The light-curve of PACN-01-04 contains six points before the observed maximum of  $r' = 17.90 \pm 0.03$  at 4:25 on 27<sup>th</sup> August 2001. It was first observed at on 24<sup>th</sup> August at 1.9 magnitudes below peak and was followed for about two magnitudes after its maximum light. PACN-00-05 was first observed on 4th August 2000, during the second season. Its maximum observed brightness was  $r' = 17.58 \pm 0.03$ . A secondary maximum of  $r' = 19.59 \pm 0.03$  occurred about 500 days after maximum light following a transition phase. Unfortunately the transition phase occurred between the end of the second season and the start of the third, so no information is available for this nova during this phase. The nova was followed through two magnitudes before the end of the second season.

The CN PACN-01-06 was also discovered by the Naini Tal microlensing group (Joshi et al. 2004), and was designated CN NMS-2 by them.

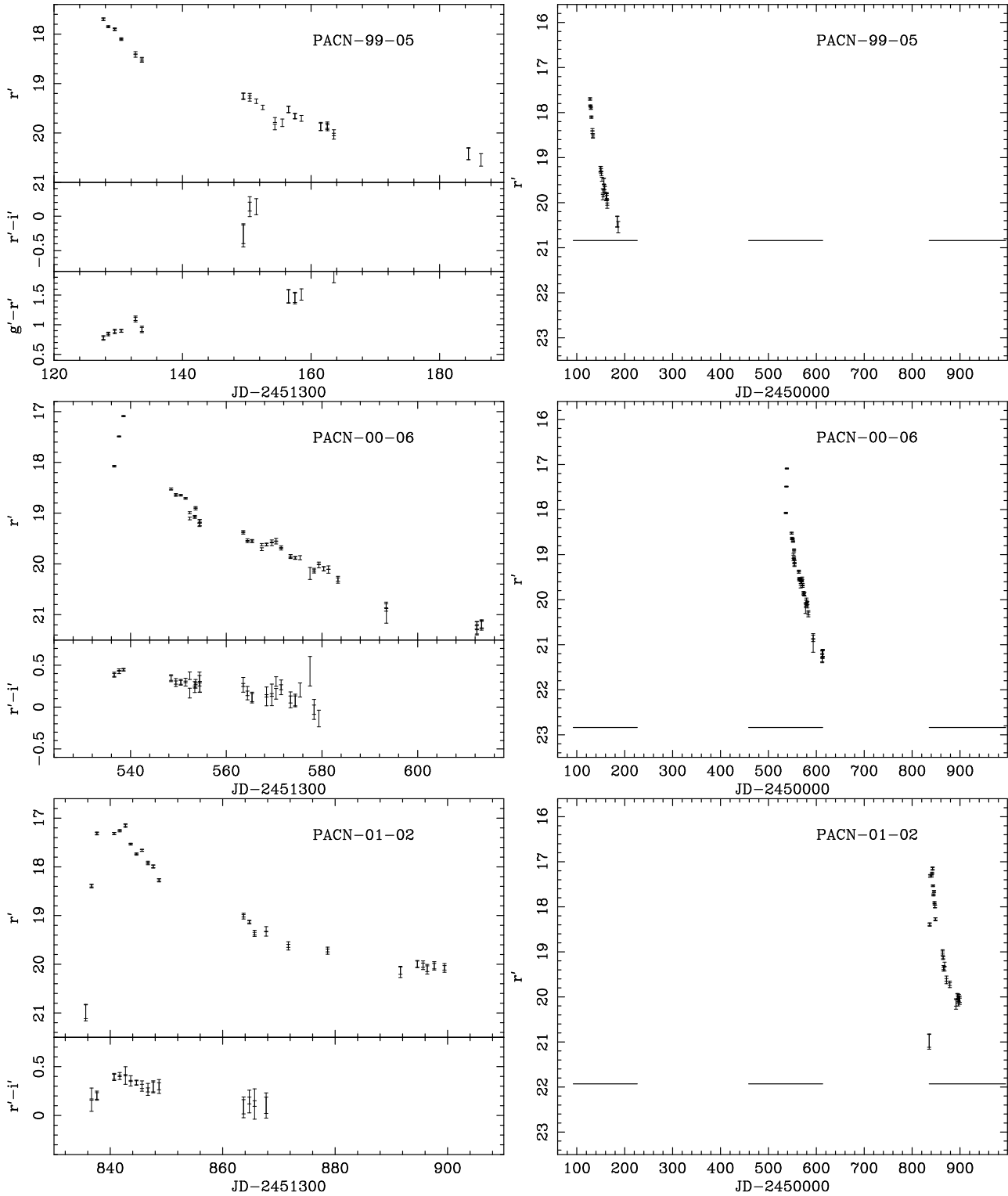
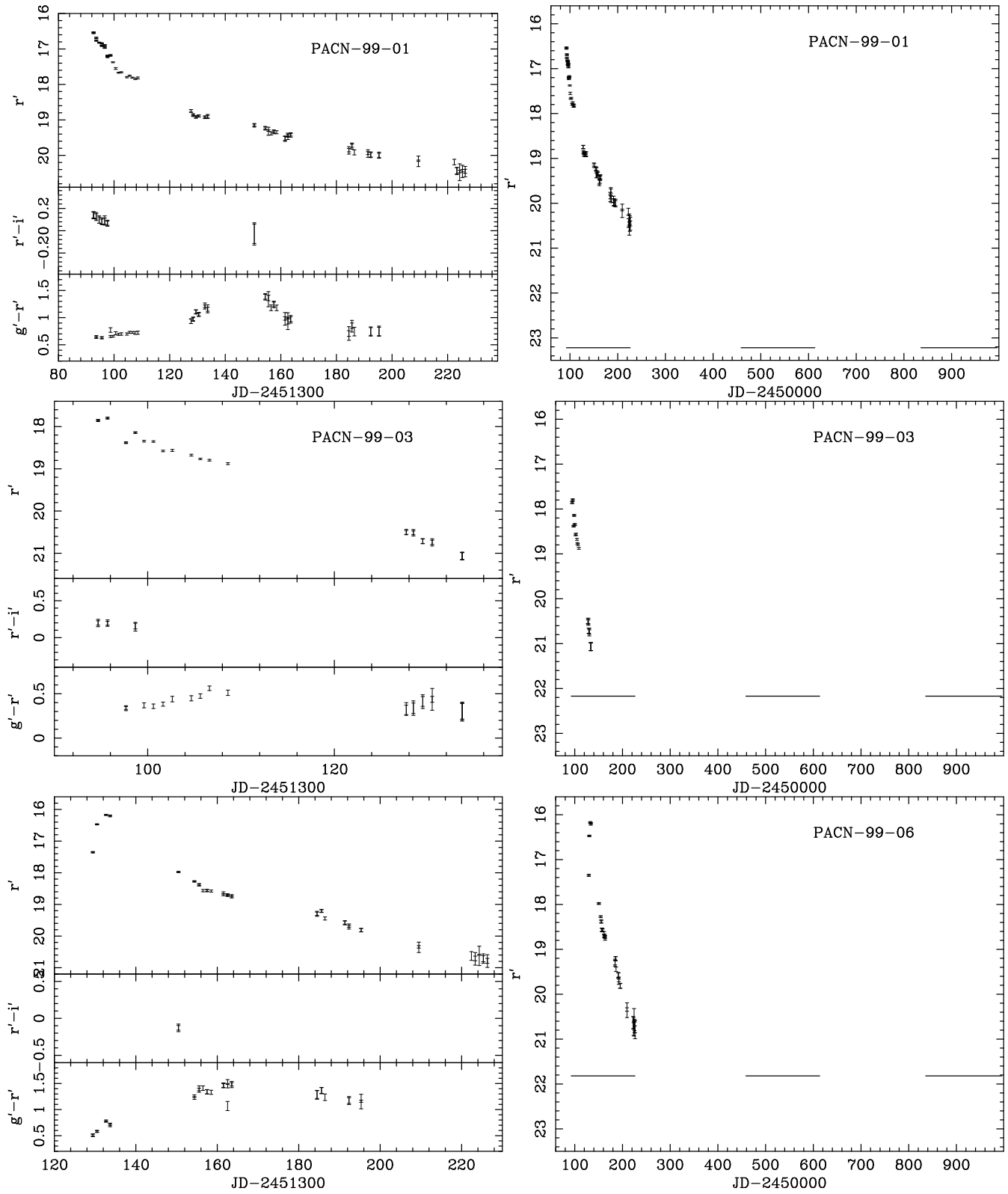


Figure 6. Fast novae in the POINT-AGAPE dataset. The panels are as for Figure 5.

We are less certain about the classification of PACN-00-07 as a CN. At first glance it looks very much like that of a CN. The rate of decline indicates that it is a moderately fast nova. However with a maximum magnitude of  $r' = 19.53 \pm 0.04$  it is much fainter than the other ten moderately fast CNe which all have maximum light in the range  $r' = 15.9$  to  $17.9$ . Interestingly, PACN-00-07's

colour evolution appears to be more like that of a Mira than of a CN (see Figure 11 for comparison), but its position on the colour-magnitude diagram (Figure 4) is much nearer to the CNe group than that of the other objects (see Section 5.8). Perhaps tellingly, it is the object which lies closest to the dividing line between the groups in a position which is suggestive of a significant extinction effect ( $\sim$



**Figure 7.** Moderately fast novae in the POINT-AGAPE dataset. The panels are as for Figure 5.

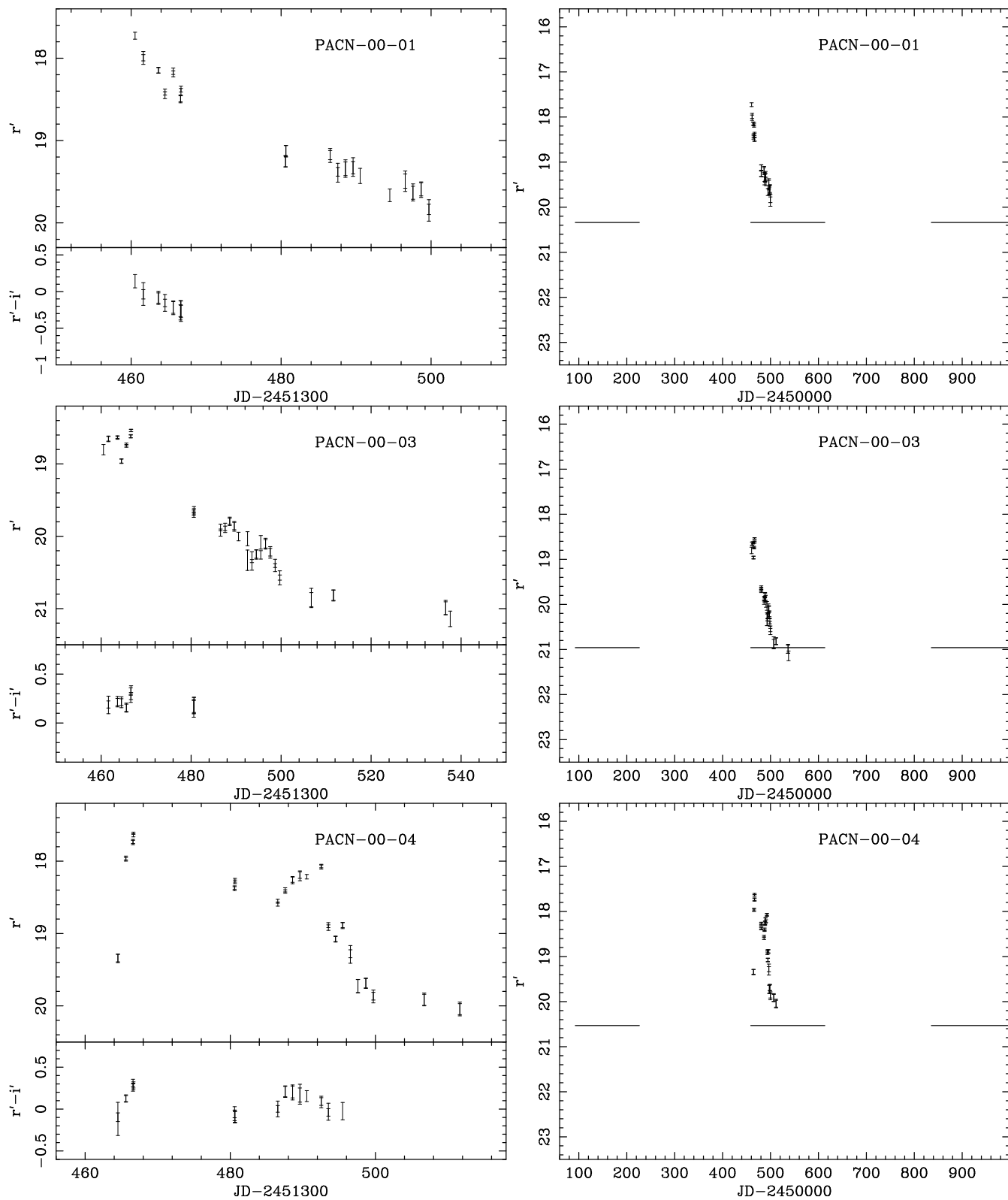


Figure 7. continued.

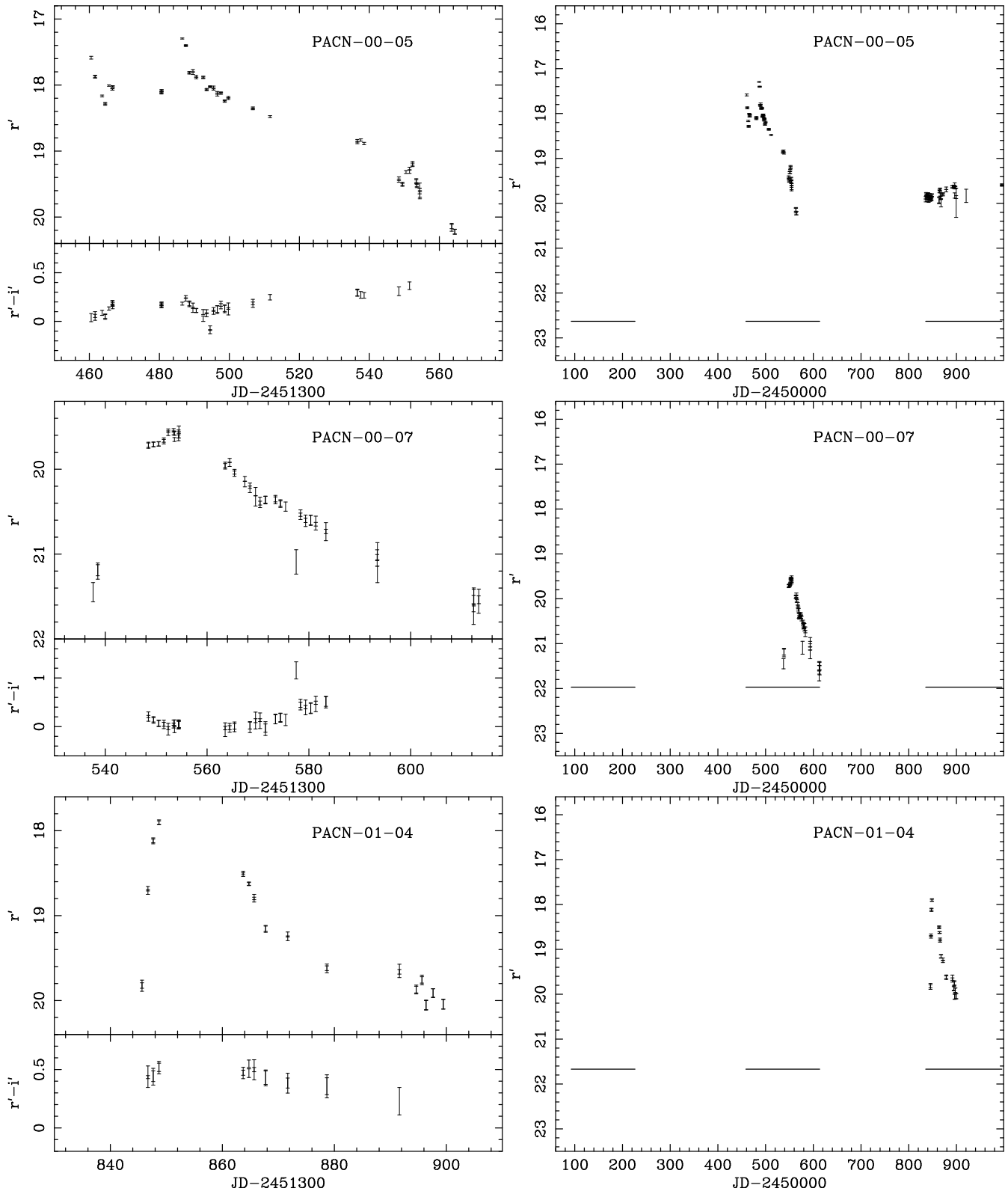


Figure 7. continued.

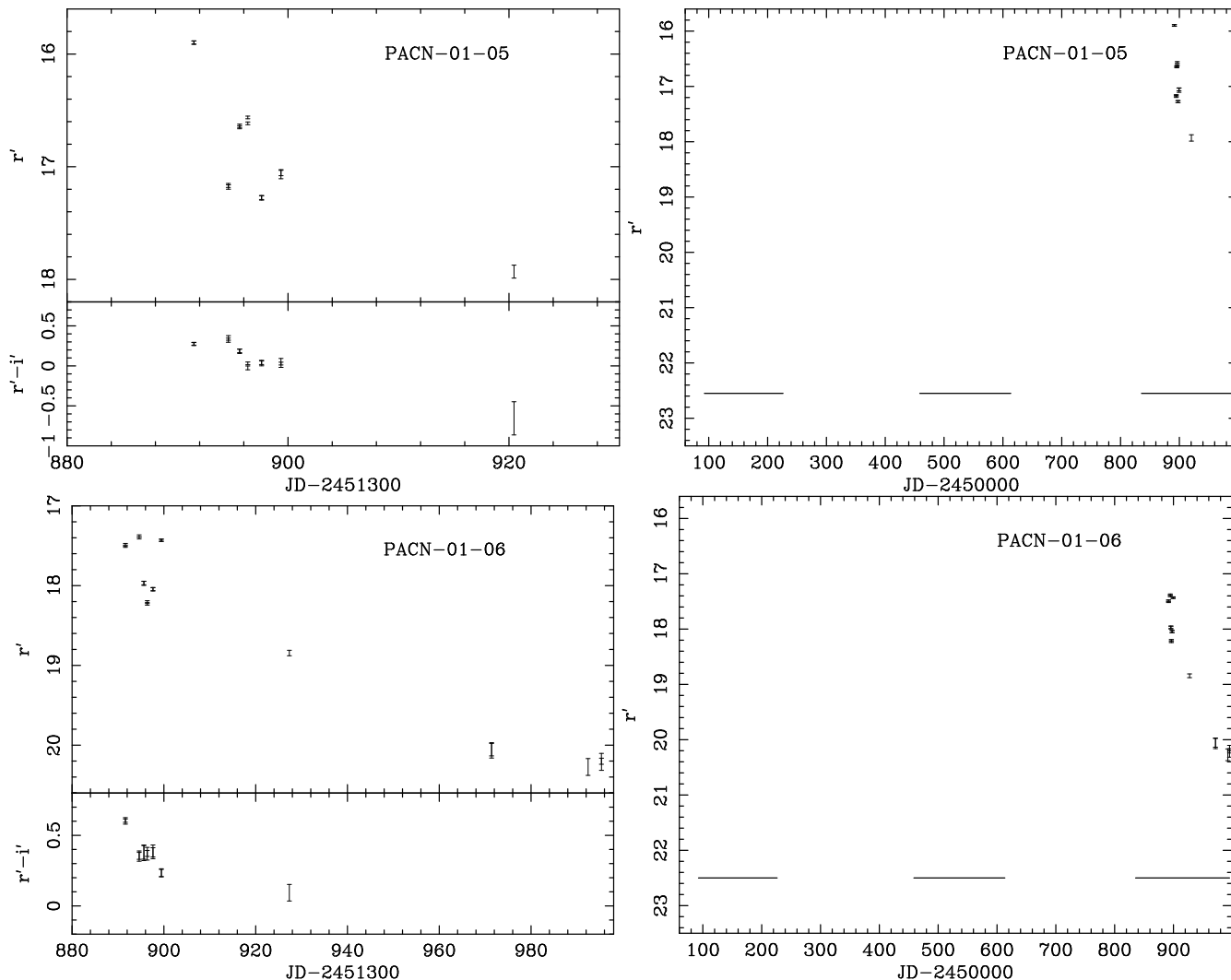


Figure 7. continued.

1 – 2 magnitudes in  $r'$ ). It is possible that PACN-00-07 is a highly extinguished nova or that it is a CN whose maximum light occurred during the gap between the 1st and 2nd season, and we are just observing a local maximum in the light-curve. Conceivably, this object could be a recurrent CN or perhaps an X-ray nova, though these properties would not necessarily result in a fainter maximum than expected for “regular” CN, and a search for possible X-ray counterparts in the Nasa Extragalactic Database (NED) reveals no matching candidates. In our view the most probable explanation is that the light from this CN is attenuated by dust.

#### 5.4 Slow novae

Three slow novae were discovered, with a  $dr'/dt$  of 0.013 – 0.024 mag day<sup>-1</sup>, and are displayed in Figure 8. Two of these slow CNe, PACN-99-04 and PACN-01-03, were first observed during their final rise phase. However, as slow novae are generally fainter than the fast novae (at maximum light), it was not possible to follow either PACN-99-02 or PACN-99-04 into their transition stage. PACN-01-03, although somewhat brighter, occurred at the end of the third season.

PACN-99-04 was first observed on 4th August 1999, the first

epoch of the 1st season, with  $r' = 18.84 \pm 0.04$ . The maximum light was observed on 9th August with  $r' = 18.41 \pm 0.03$ . The nova was followed for about 2 magnitudes below peak.

The CN PACN-01-03 was observed seventeen times throughout its final rise phase. This nova was first observed with  $r' = 19.27 \pm 0.08$  and rose steadily for 8 days to its observed maximum of  $r' = 17.30 \pm 0.04$  on 27th August 2001. We were only able to follow this nova during its initial decline phase for around two magnitudes before the end of the third season.

#### 5.5 Very slow novae

As shown in Figure 9, we discovered two very slow CNe. Very slow CNe take 151 – 250 days to decrease by two magnitudes from maximum light.

The maximum in the  $r'$ -band light-curve of PACN-00-02 was observed at the beginning of the second season on 4th August 2000 and the nova was still clearly visible by the end of the second season on 3rd January 2001. However, it had become unresolved by the beginning of the third. This CN reached an observed maximum light of  $r' = 18.15 \pm 0.03$  and had diminished by only 1.8 magnitudes by the end of the second season, 150 days later, with an

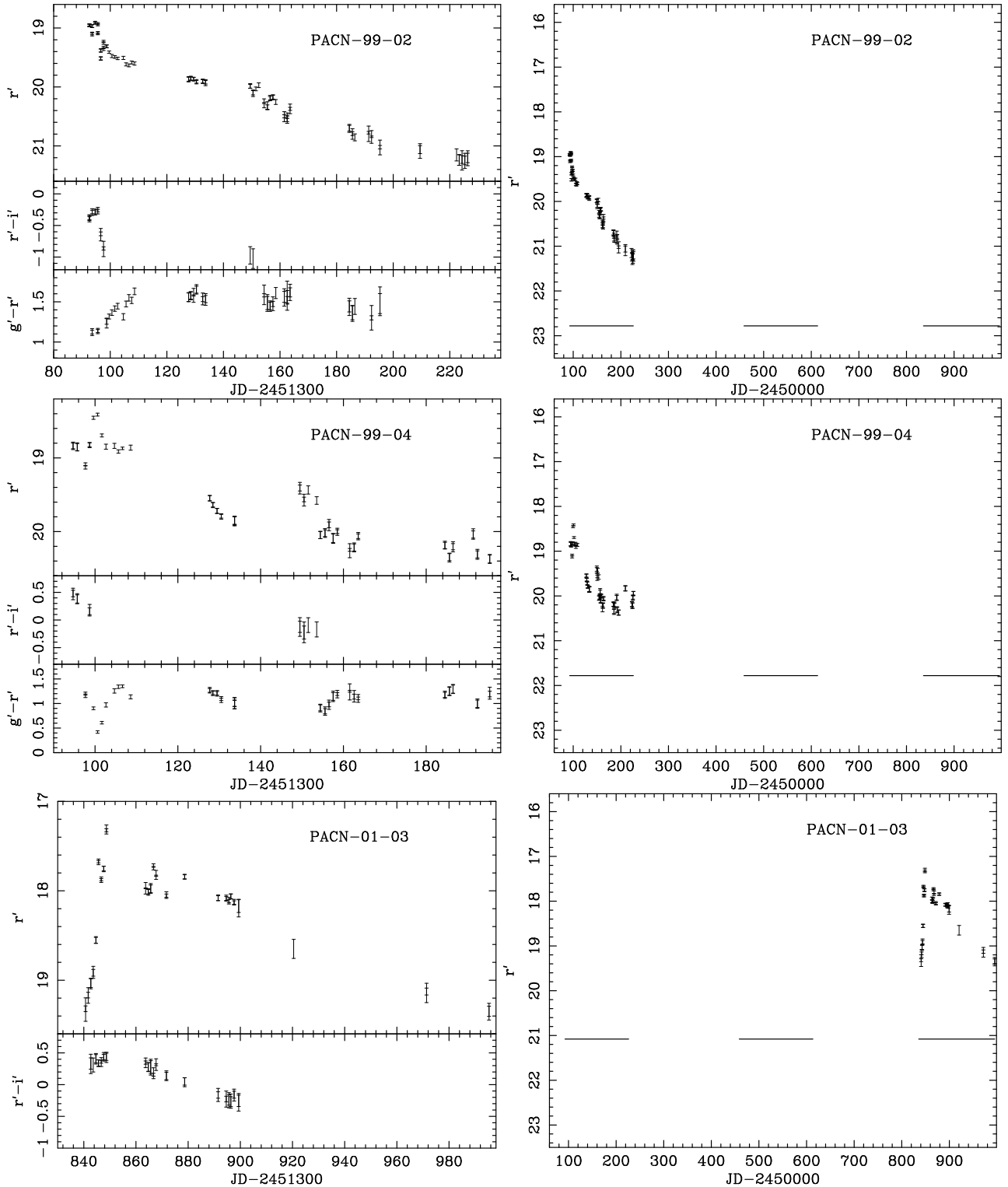


**Figure 8.** Slow novae in the POINT-AGAPE dataset. The panels are as for Figure 5.

estimated  $dr'/dt \simeq 0.01 \text{ mag day}^{-1}$ . PACN-00-02 has a relatively smooth light-curve, except for a feature about 100 days after maximum light in which the nova brightened by about a third of a magnitude, before continuing to decline again.

PACN-01-01 is an interesting object, though we have some reservations over its classification as a nova. It was not possible

to sample enough of PACN-01-01's light-curve to make a reliable measurement of  $dr'/dt$  as this nova remained around maximum-light for the majority of the time that it was observed. Its speed class, if it is a CN, is therefore uncertain. However, it has passed all of our selection criteria. The 3rd season data are similar in some respects to the structure around maximum light of the light-curves of



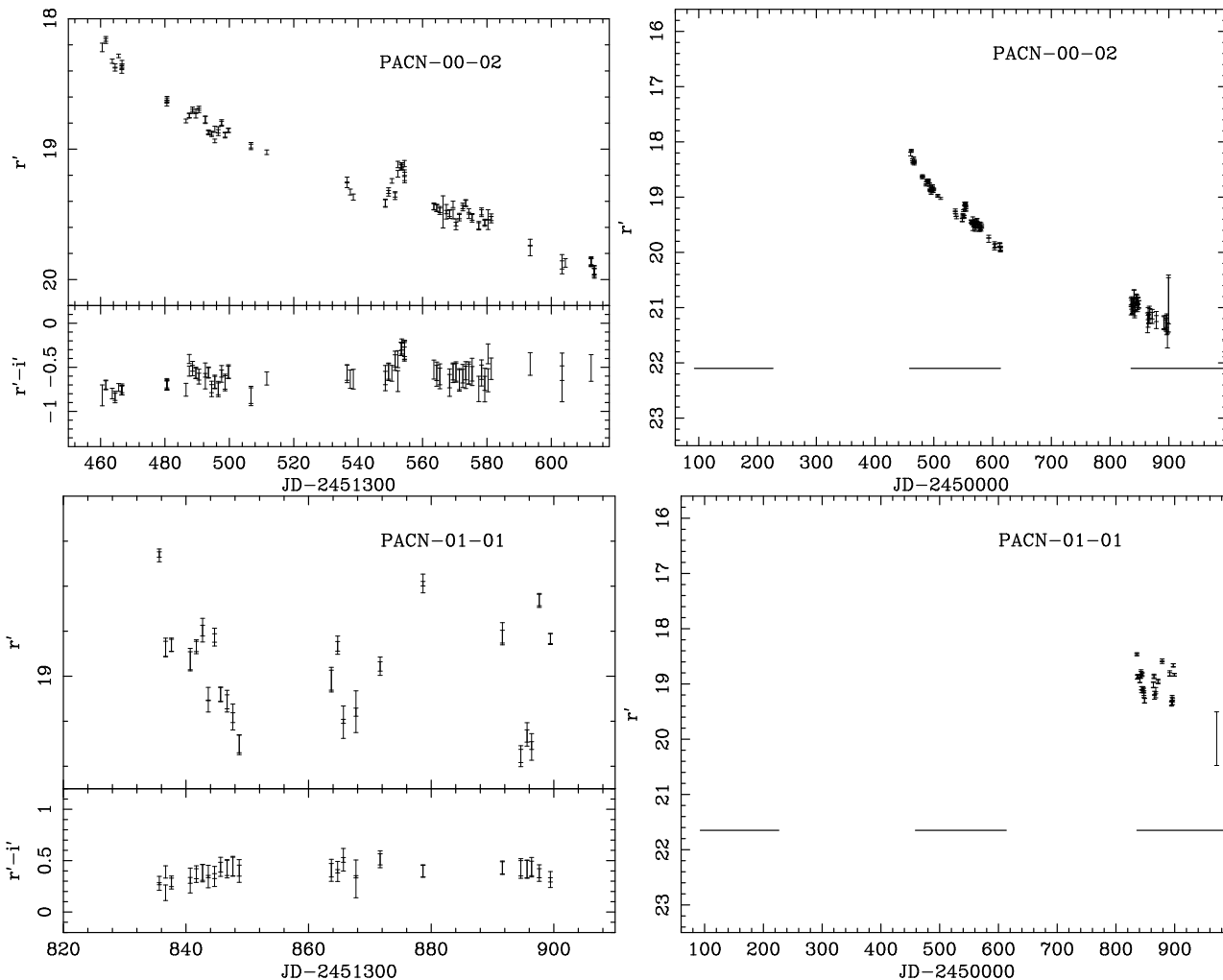


Figure 9. Very slow novae in the POINT-AGAPE dataset. The panels are as for Figure 5.

some of the moderately fast (DQ Her-like) novae in this catalogue, e.g. PACN-00-04 and PACN-00-05. However, there may be a more marked similarity to the light-curve around maximum of the very slow nova HR Del 1967 (Drechsel et al. 1977). We also note that PACN-01-01 is only 3 arcmin from the centre of M31 and hence suffers significantly from a highly variable background. The points in the 1st and 2nd seasons likely arise from a statistical anomaly in the M31 background at or close to the position of this nova, and are not related to the outburst in the 3rd season, as no resolved object is visible at this location.

### 5.6 Distribution of classical novae

The distribution of candidates with CCD can be seen in Table 8. Figure 10 gives a graphical representation of each candidate’s position within our fields. The distribution shows some evidence of spatial concentration around the bulge, however we caution that the significance of this cannot be properly estimated before we make Monte-Carlo completeness tests of our selection criteria, something which we will report in a follow-up paper. One nova (PACN-00-07) lies well outside the main disk light on the far-disk side of M31. If it is associated with the M31 disk then it must lie at a de-projected distance of around 25 kpc from the centre of M31, or around 4 disk scale lengths.

Table 8. The distribution within each CCD of candidates selected by our classical nova detection pipeline.

CCD	Candidates	Percentage of total
North 1	4	20.0%
North 2	4	20.0%
North 3	1	5.0%
North 4	3	15.0%
South 1	0	0.0%
South 2	0	0.0%
South 3	6	30.0%
South 4	2	10.0%

As can be seen from Figure 10, one of our CNe may be located within the dwarf spheroidal galaxy M32. This nova, PACN-99-04, is located 22.6 arcmin from the centre of M31, but is only 1.8 arcmin from the centre of M32.

### 5.7 Pipeline detection efficiency

In a forthcoming study we shall make a careful assessment of the efficiency with which CNe are detected by our pipeline. However,

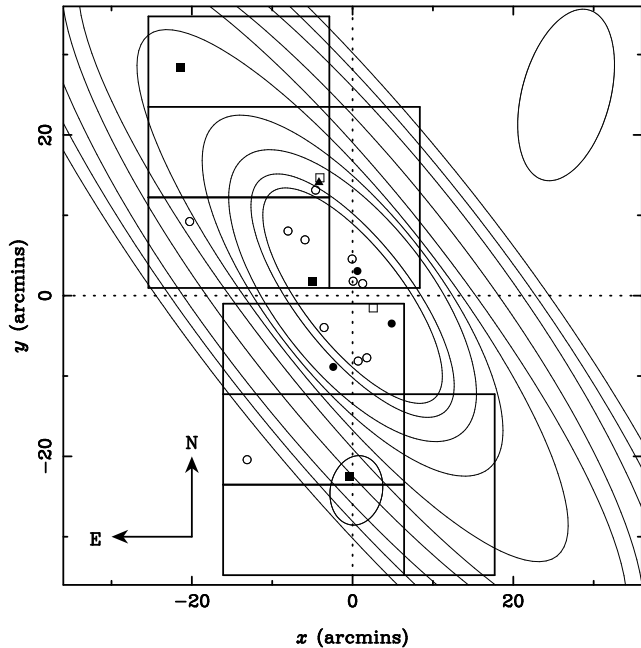


**Figure 10.** The positions of the selected classical nova candidates within M31. The lines and contours are as for Figure 1. The different symbols indicate a very fast nova (solid triangle), fast novae (closed circles), moderately fast novae (open circles), slow novae (closed boxes), and very slow novae (open boxes).

a useful comparison can be made with the CNe which have been announced on IAU Circulars during the lifetime of the survey. An et al. (2004) found that 12 of the 14 CN which were alerted during our survey are present in the POINT-AGAPE dataset. All of these CNe are located within a few arcmins of the centre of M31 and are of fast or moderately fast speed class. Our automated pipeline has identified 7 out of the 12 CNe listed in Table 3 of An et al. (2004). Of the remaining five, two (26285/26121 and 79136, using the An et al. identifiers) occur too late in the survey to be properly sampled (and therefore failed selection). One CN (78668) was lost due to our image trimming as it occurs close to the northern edge of CCD3 in the southern field. Another (83479) was lost due to the masking of a diffraction spike of a very bright star, and the final missed CN (26277/25695) failed the initial  $15\sigma$  cut. We therefore conclude that our pipeline successfully recognises CNe within the boundaries of our defined selection criteria.

### 5.8 Borderline and other light-curves

From the inspection of the CN in our catalogue, we are confident that at least 18 of the candidates are CNe. However there are two CN, PACN-00-07 and PACN-01-01, that we are less certain about.

As shown in Table 5, thirty-two CN candidates were eliminated only by the two colour-magnitude criteria. As can be seen in Figure 4, these candidates appear to be located in a “clump”, indicating that they may be similar types of object. From inspection, the majority of these candidates appear to be Miras or Mira-like variables, with a few exceptions. Figure 11, shows the light-curve of the brightest Mira discovered. Its position in the colour-magnitude diagram is indicated in Figure 4. This object exhibits a very smooth light-curve and its position ( $\alpha = 0^{\text{h}}44^{\text{m}}23^{\text{s}}.7, \delta = +41^{\circ}28'4''$ ) is coincident with an object exhibiting a remarkably similar light-curve from the DIRECT survey (Stanek et al. 1999), V9205 D31C,

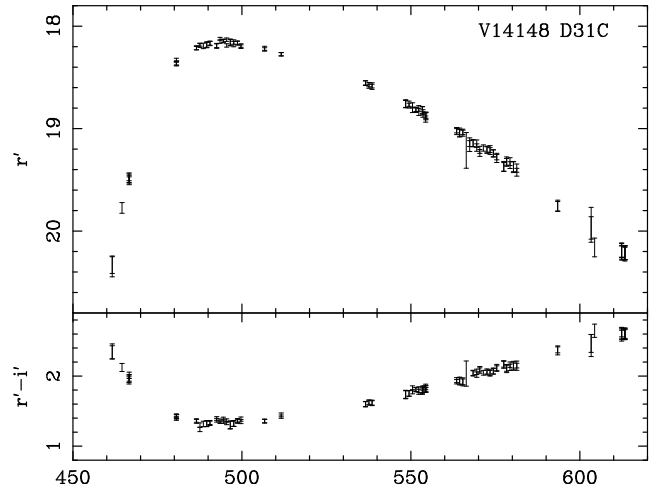


**Figure 11.** Mira variable V9205 D31C as observed by our survey.

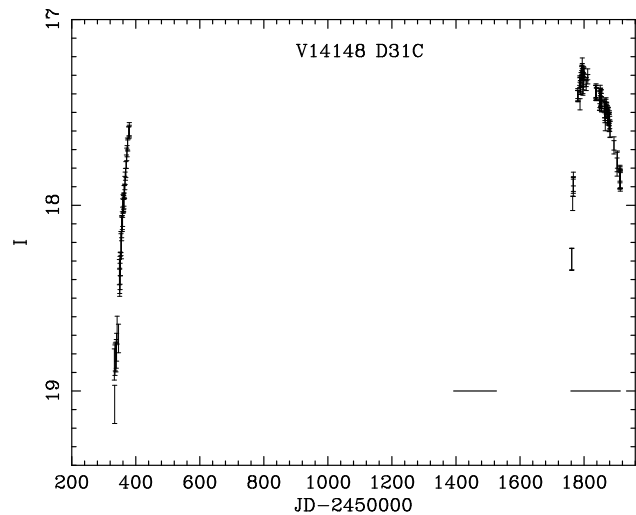


**Figure 12.** Mira variable V9205 D31C. Earlier data from the DIRECT survey (Stanek et al. 1999), later data from this survey. The horizontal lines indicate the length of the 1st and 2nd POINT-AGAPE observing seasons.

observed between September and October 1996. Figure 12 shows both the DIRECT *I*-band data and POINT-AGAPE data that has been transformed into *I*-band data, as well as the span of the 1st and 2nd POINT-AGAPE observing seasons. The transformation of the POINT-AGAPE data to the *I* band is obtained by deriving a best-fit linear transformation from  $i'$  and  $r'$  to *I* using the Magnier et al. (1992) standard stars. From a simple analysis of the DIRECT and POINT-AGAPE data, given that the Mira was unresolved throughout the 1st POINT-AGAPE season, we arrive at two possible periods for this Mira, either  $\sim 700$  days or  $\sim 1400$  days, making it one of the longest period Miras observed. At the distance of M31, it is also one of the most luminous.

The high signal-to-noise ratio microlensing event PA-99-N2 (Paulin-Henriksson et al. 2003) was also identified and was eliminated from the catalogue via the colour evolution selection criterion (as would be expected for a strong microlensing event). The light-curve of the event produced using the CN detection pipeline is shown in Figure 13. A recent detailed analysis of this event using “superpixel” photometry indicates anomalies near the peak of the light-curve which are well explained as being due to a binary lens

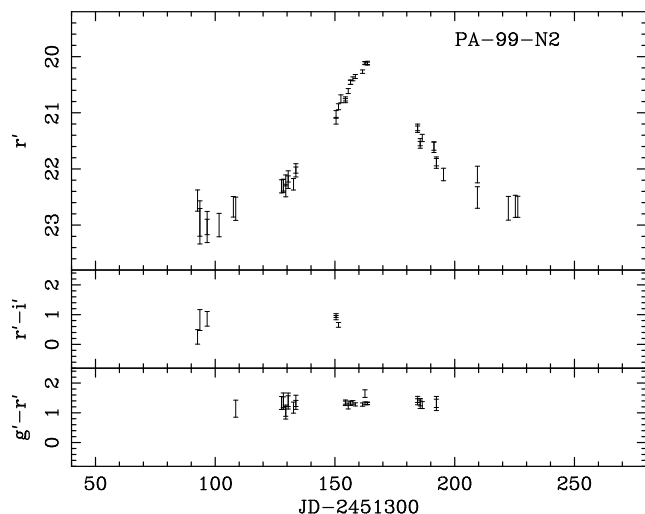


**Figure 13.** The PSF-fitted light-curve of the microlensing event PA-99-N2 discovered previously by Paulin-Henriksson et al. (2003) using “superpixel” photometry. The event is investigated in detail by An et al. (2004).

system (An et al. 2004). The PSF-fitting photometry independently undertaken for this study confirms the anomalous kink on an otherwise smooth and achromatic light-curve, occurring on the rising side near peak.

## 6 CONCLUSIONS

The primary aim of the POINT-AGAPE survey is to search for microlensing events due to compact dark matter in M31. However, the requirements for such a survey also enable us to compile a substantial catalogue of variable stars and transients. In this study we have conducted the first fully-automated search for classical novae (CNe), using objective selection criteria to define our sample. Our aim has been to devise criteria which, as far as possible, do not bias against the detection of CNe of certain speed classes in favour of others, despite the difficulty that the CN light-curve morphology is inextricably linked to its speed class. In the absence of  $H\alpha$  observations, which are an important diagnostic for CN identification, excellent sampling is a crucial pre-requisite for this task.

Our final catalogue of 20 CNe obtained from 3 seasons of data covering 18 months of total observing time spans a wide range of speed class from very fast to very slow. Their light-curve morphologies vary considerably from the smoothly declining very slow CN, PACN-00-02, through to the moderately fast CN, PACN-00-05, which exhibits multiple maxima as well as a deep transition minimum. Among the objects which did not make our catalogue is V9205 D31C, first seen by the DIRECT survey (Stanek et al. 1999). Combining the DIRECT data and POINT-AGAPE data reveals this object to be a Mira with a period of either 700 or 1400 days, making it one of the longest-period and (if as seems most likely it lies in M31) most luminous Miras known. Our PSF-fitting photometry also confirms the anomalous behaviour of the high signal-to-noise ratio microlensing event PA-99-N2 (An et al. 2004), first discovered using our “superpixel” photometry pipeline. Overall, despite the absence of  $H\alpha$  data, we are confident that most, if not all, of our sample are indeed CNe. The only possible borderline candidates are PACN-00-07 and PACN-01-01.

In a follow-up study we intend to use our CN catalogue to undertake an objective study of the spatial and speed class distribu-

tion of CNe in M31. This may help to answer key questions such as whether there is more than one population of CN and whether CNe of different speed classes tend to be associated with different stellar populations. From Monte-Carlo completeness tests we should be able to assess objectively the underlying global nova rate, the spatial distribution of CNe, and their potential as standard candle distance estimators via the maximum-magnitude versus rate-of-decline and other relationships. The detailed profiles observed for several of the novae, especially prior to maximum, may also prove helpful for constraining theoretical models of the nova outburst.

## ACKNOWLEDGEMENTS

The work of MJD and MFB is supported by a studentship and a Senior Fellowship respectively from the Particle Physics and Astronomy Research Council. JA is supported by a grant from the Leverhulme Trust Foundation and NWE thanks the Royal Society for support. SCN is supported by the Swiss National Science Foundation and the Tomalla Foundation.

This research has made use of the NASA/IPAC Extragalactic Database (NED) which is operated by the Jet Propulsion Laboratory, California Institute of Technology, under contract with the National Aeronautics and Space Administration.

This research has made use of the SIMBAD database, operated at CDS, Strasbourg, France.

## REFERENCES

- Adams W. S., Joy A. H., 1936, *ApJ*, 84, 14
- An J., Evans N., Hewett P., Baillon P. and Calchi-Novati S., Carr B. J., Cr ez e M., Giraud-H eraud Y., Gould A., Jetzer P., Kaplan J., Kerins E., Paulin-Henriksson S., Smartt S. J., Stalin C., Tsapras Y., 2004, *MNRAS*, in press
- An J. H., Evans N. W., Kerins E., Baillon P., Calchi Novati S., Carr B. J., Cr ez e M., Giraud-H eraud Y., Gould A., Hewett P., Jetzer P., Kaplan J., Paulin-Henriksson S., Smartt S. J., Tsapras Y., Valls-Gabaud D., 2004, *ApJ*, 601, 845
- Arp H. C., 1956, *AJ*, 61, 15
- Bertaud C., 1948, *Annales d’Astrophysique*, 11, 3
- Bode M. F., Evans A., 1989, *Classical novae*. Chichester: Wiley, 1989, edited by Bode, M.F.; Evans, A.
- Buscombe W., de Vaucouleurs G., 1955, *The Observatory*, 75, 170
- Capaccioli M., della Valle M., Rosino L., D’Onofrio M., 1989, *AJ*, 97, 1622
- Ciardullo R., Ford H., Jacoby G., 1983, *ApJ*, 272, 92
- Ciardullo R., Ford H. C., Neill J. D., Jacoby G. H., Shafter A. W., 1987, *ApJ*, 318, 520
- Ciardullo R., Shafter A. W., Ford H. C., Neill J. D., Shara M. M., Tomaney A. B., 1990, *ApJ*, 356, 472
- Ciardullo R., Tamblyn P., Jacoby G. H., Ford H. C., Williams R. E., 1990, *AJ*, 99, 1079
- Crane P. C., Dickel J. R., Cowan J. J., 1992, *ApJL*, 390, L9
- Crawford J. A., Kraft R. P., 1956, *ApJ*, 123, 44
- Darnley M. J., Bode M. F., Kerins E. J., O’Brien T. J., 2002, in *AIP Conf. Proc. 637: Classical Nova Explosions Novae In External Galaxies From The POINT-AGAPE Survey And The Liverpool Telescope*. pp 481–485
- de Vaucouleurs G., 1958, *ApJ*, 128, 465
- Drechsel H., Rahe J., Duerbeck H. W., Kohoutek H. W., Seitter W. C., 1977, *A&AS*, 30, 323

- Duerbeck H. W., 1981, *PASP*, 93, 165
- Haiman Z., Magnier E., Lewin W. H. G., Lester R. R., van Paradijs J., Hasinger G., Pietsch W., Supper R., Truemper J., 1994, *A&A*, 286, 725
- Hubble E. P., 1929, *ApJ*, 69, 103
- Joshi Y. C., Pandey A. K., Narasimha D., Giraud-Héraud Y., Sagar R., Kaplan J., 2004, *A&A*, 415, 471
- Kerins E., Carr B. J., Evans N. W., Hewett P., Lastennet E., Le Du Y., Melchior A.-L., Smartt S. J., Valls-Gabaud D., 2001, *MNRAS*, 323, 13
- King A. R., 1989, in Bode M. F., Evans A., eds, *Classical novae*. Chichester: Wiley, pp 17–37
- Magnier E. A., Lewin W. H. G., van Paradijs J., Hasinger G., Jain A., Pietsch W., Truemper J., 1992, *A&AS*, 96, 379
- McLaughlin D. B., 1939, *Popular Astronomy*, 47, 410
- McLaughlin D. B., 1941, *PASP*, 53, 102
- McLaughlin D. B., 1945, *PASP*, 57, 69
- McLaughlin D. B., 1960. *Stellar atmospheres* Edited by J. L. Greenstein, published by University of Chicago Press
- Paulin-Henriksson S., Baillon P., Bouquet A., Carr B. J., Crézé M., Evans N. W., Giraud-Héraud Y., Gould A., Hewett P., Kaplan J., Kerins E., Le Du Y., Melchior A.-L., Smartt S. J., Valls-Gabaud D., 2003, *A&A*, 405, 15
- Payne-Gaposchkin C. H., 1957, *The galactic novae*. Amsterdam, North-Holland Pub. Co.; New York, Interscience Publishers, 1957.
- Rector T. A., Jacoby G. H., Corbett D. L., Denham M., RBSE Nova Search Team 1999, *Bulletin of the American Astronomical Society*, 31, 1420
- Rosino L., 1964, *Annales d’Astrophysique*, 27, 498
- Rosino L., 1973, *A&AS*, 9, 347
- Rosino L., Capaccioli M., D’Onofrio M., della Valle M., 1989, *AJ*, 97, 83
- Shafter A. W., 1997, *ApJ*, 487, 226
- Shafter A. W., Irby B. K., 2001, *ApJ*, 563, 749
- Shara M. M., 1981, *ApJ*, 243, 268
- Sharov A. S., 1972, *Soviet Astronomy*, 16, 41
- Sharov A. S., Alksnis A., 1991, *Astrophysics and Space Science*, 180, 273
- Stanek K. Z., Kaluzny J., Krockenberger M., Sasselov D. D., Tonry J. L., Mateo M., 1999, *AJ*, 117, 2810
- Starrfield S., 1989, in Bode M. F., Evans A., eds, *Classical novae*. Chichester: Wiley, pp 39–60
- Tomaney A. B., Shafter A. W., 1992, *ApJS*, 81, 683
- van den Bergh S., Younger P. F., 1987, *A&AS*, 70, 125
- Warner B., 1989, in Bode M. F., Evans A., eds, *Classical novae*. Chichester: Wiley, pp 1–16

**Table 6.** The POINT-AGAPE classical nova catalogue.  $x$  and  $y$  are the positions from the M31 centre measured in arcminutes along the M31 major and minor axis, respectively. The epoch  $t_0(r')$  is the time of the brightest  $r'$ -band observation. The maximum magnitudes  $r'(t_0)$ ,  $i'(t_0)$  and  $g'(t_0)$  are the brightest observed magnitude in each band.  $dr'/dt$  is an estimate of the rate of decline between the brightest observation and the observation closest to 2 magnitudes fainter than the maximum observed. The speed class is estimated by assuming the  $V$ -band definition in Table 2 also holds for our  $r'$ -band data.

Nova	R.A. (J2000)	Decl. (J2000)	$x$ (arcmin)	$y$ (arcmin)	$t_0(r')$ JD-2451000	$r'(t_0)$	$i'(t_0)$	$g'(t_0)$	$dr'/dt$ (mag day <sup>-1</sup> ) (estimate)	Speed class
PACN-99-01	0 <sup>h</sup> 43 <sup>m</sup> 27 <sup>s</sup> .2	+41°24'11''.1	-8.0	8.0	392.63	16.53 ± 0.03	16.39 ± 0.03	17.40 ± 0.01	0.06	Moderately Fast
PACN-99-02	0 <sup>h</sup> 44 <sup>m</sup> 39 <sup>s</sup> .2	+41°44'32''.4	-21.4	28.4	394.65	18.91 ± 0.03	19.19 ± 0.04	20.22 ± 0.02	0.02	Slow
PACN-99-03	0 <sup>h</sup> 42 <sup>m</sup> 34 <sup>s</sup> .9	+41°08'24''.5	1.8	-7.7	395.71	17.79 ± 0.02	17.60 ± 0.04	-	0.03	Moderately Fast
PACN-99-04	0 <sup>h</sup> 42 <sup>m</sup> 46 <sup>s</sup> .1	+40°53'35''.3	-0.3	-22.6	400.61*	18.41 ± 0.02	18.34 ± 0.07	18.83 ± 0.02	0.02	Slow
PACN-99-05	0 <sup>h</sup> 42 <sup>m</sup> 41 <sup>s</sup> .1	+41°19'12''.2	0.6	3.1	427.69	17.70 ± 0.04	-	18.47 ± 0.02	0.02	Fast
PACN-99-06	0 <sup>h</sup> 43 <sup>m</sup> 15 <sup>s</sup> .9	+41°23'05''.4	-5.9	6.9	432.69*	16.17 ± 0.01	-	16.91 ± 0.01	0.06	Moderately Fast
PACN-99-07	0 <sup>h</sup> 43 <sup>m</sup> 06 <sup>s</sup> .7	+41°30'14''.2	-4.2	14.1	484.50	18.1 ± 0.1	18.02 ± 0.04	18.5 ± 0.1	0.2	Very Fast
PACN-00-01	0 <sup>h</sup> 42 <sup>m</sup> 44 <sup>s</sup> .0	+41°17'56''.5	0.1	1.8	760.52	17.73 ± 0.04	17.58 ± 0.8	-	0.05	Moderately Fast
PACN-00-02	0 <sup>h</sup> 43 <sup>m</sup> 06 <sup>s</sup> .0	+41°30'48''.3	-4.1	14.7	761.63	18.15 ± 0.03	18.86 ± 0.05	-	0.01	Very Slow
PACN-00-03	0 <sup>h</sup> 42 <sup>m</sup> 44 <sup>s</sup> .6	+41°20'42''.1	-0.1	4.6	766.64	18.54 ± 0.03	18.19 ± 0.04	-	0.06	Moderately Fast
PACN-00-04	0 <sup>h</sup> 42 <sup>m</sup> 37 <sup>s</sup> .6	+41°17'38''.6	1.3	1.5	766.65*	17.61 ± 0.03	17.33 ± 0.04	-	0.07	Moderately Fast
PACN-00-05	0 <sup>h</sup> 43 <sup>m</sup> 08 <sup>s</sup> .9	+41°29'16''.6	-4.6	13.1	786.54	17.30 ± 0.01	17.11 ± 0.01	-	0.03	Moderately Fast
PACN-00-06 <sup>a</sup>	0 <sup>h</sup> 42 <sup>m</sup> 57 <sup>s</sup> .1	+41°07'16''.3	-2.4	-8.9	838.52*	17.09 ± 0.01	16.64 ± 0.01	-	0.1	Fast
PACN-00-07	0 <sup>h</sup> 43 <sup>m</sup> 53 <sup>s</sup> .8	+40°55'43''.5	-13.1	-20.4	854.46*	19.53 ± 0.04	19.48 ± 0.05	-	0.03	Moderately Fast
PACN-01-01	0 <sup>h</sup> 42 <sup>m</sup> 30 <sup>s</sup> .6	+41°14'36''.8	2.6	-1.5	1135.64	18.45 ± 0.02	18.16 ± 0.04	-	0.01	Very Slow
PACN-01-02	0 <sup>h</sup> 42 <sup>m</sup> 18 <sup>s</sup> .4	+41°12'40''.3	4.9	-3.5	1142.71*	17.14 ± 0.03	16.71 ± 0.04	-	0.09	Fast
PACN-01-03	0 <sup>h</sup> 43 <sup>m</sup> 10 <sup>s</sup> .6	+41°17'57''.6	-4.9	1.8	1148.67*	17.30 ± 0.04	16.88 ± 0.06	-	0.01	Slow
PACN-01-04	0 <sup>h</sup> 42 <sup>m</sup> 40 <sup>s</sup> .6	+41°07'59''.9	0.7	-8.1	1148.69*	17.90 ± 0.03	17.38 ± 0.04	-	0.05	Moderately Fast
PACN-01-05	0 <sup>h</sup> 44 <sup>m</sup> 32 <sup>s</sup> .5	+41°25'21''.9	-20.3	9.2	1191.48	15.90 ± 0.01	15.61 ± 0.01	-	0.07	Moderately Fast
PACN-01-06 <sup>b</sup>	0 <sup>h</sup> 43 <sup>m</sup> 03 <sup>s</sup> .2	+41°12'10''.5	-3.5	-4.0	1194.62*	17.38 ± 0.01	16.88 ± 0.03	-	0.04	Moderately Fast

<sup>a</sup> CN NMS-1 (Joshi et al. 2003).

<sup>b</sup> CN NMS-2 (Joshi et al. 2003).

\* these novae have been observed before maximum-light, in their final rise phase.